Spin wave eigenmodes in transversely magnetized thin film ferromagnetic wires

Zheng Duan[*] and Ilya N. Krivorotov

Department of Physics and Astronomy, University of California, Irvine, California 92697, USA

Rodrigo E. Arias

Departamento de Física, FCFM, Universidad de Chile, Casilla 487-3, Santiago, Chile

Nathalie Reckers

Experimentalphysik - AG Farle, Fakultät für Physik and Center for Nanointegration (CeNIDE), Universität Duisburg-Essen,
Lotharstrasse 1, 47048 Duisburg, Germany

Sven Stienen and Jürgen Lindner

Helmholtz-Zentrum Dresden-Rossendorf, Institute of Ion Beam Physics and Materials Research,
Bautzner Landstrasse 400, 01328 Dresden, Germany

We report experimental and theoretical studies of spin wave eigenmodes in transversely magnetized thin film Permalloy wires. Using broadband ferromagnetic resonance technique, we measure the spectrum of spin wave eigenmodes in individual wires as a function of magnetic field and wire width. Comparison of the experimental data to our analytical model and micromagnetic simulations shows that the intrinsic dipolar edge pinning of spin waves is negligible in transversely magnetized wires. Our data also quantify the degree of extrinsic edge pinning in Permalloy wires. This work establishes the boundary conditions for dynamic magnetization in transversely magnetized thin film wires for the range of wire widths and thicknesses studied, and provides a quantitative description of the spin wave eigenmode frequencies and spatial profiles in this system as a function of the wire width.

I. INTRODUCTION

Ferromagnetic nanowires is an important experimental platform for observation of magnetotransport and magneto-dynamic phenomena emerging at the nanometer length scale. Studies of these effects such as field- and current-induced domain-wall motion [1–7], domain-wall magnetoresistance [8–10], and the interaction of spin waves with nanoscale spin textures such as domain walls, vortices, and skyrmions [11–17] heavily rely on the understanding of transport and magnetization dynamics in ferromagnetic nanowires. More recently, ferromagnetic nanowires proved to be useful for studies of inverse spin Hall effect [18] and spin-orbit torques [19–22]. Furthermore, several realizations of spintronic logic gates [23–28] and spin wave guides [29] based on ferromagnetic nanowires have been recently proposed. Detailed understanding of magnetotransport and magnetodynamic effects in ferromagnetic nanowires relies on the quantitative description of spin waves in this important confined geometry.

While the spectrum of spin waves in nanowires magnetized parallel to the wire axis is well understood [30], the situation is less clear for nanowires magnetized perpendicular to the wire axis. For example, the boundary conditions describing dynamic magnetization at the nanowire edges (and therefore the spin wave eigenmode frequencies) remain to be established. The main complication in this magnetic configuration is the strong spatial nonuniformity of the demagnetizing fields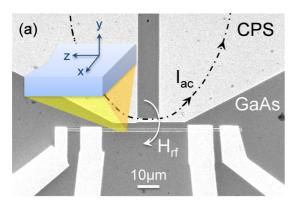, which prevents derivation of simple analytical expressions describing the spectrum of spin wave eigenmodes. This task is especially difficult when both the exchange and the dipole-dipole interactions significantly contribute to the spin wave energies [31,32].

In this paper, we describe experimental and theoretical studies of spin waves in thin film ferromagnetic wires that are magnetized transversely to the wire axis in the plane of the film. In order to simplify the problem, we choose ferromagnetic wires made of Permalloy (Py $\equiv$ Ni$_{80}$Fe$_{20}$) which has a negligible bulk magnetic anisotropy. We use the resistively detected broadband ferromagnetic resonance (FMR) technique [22,33–37] to measure the spectrum of spin wave eigenmodes in individual wires as a function of transverse magnetic field. This technique eliminates inhomogeneous broadening and interwire interaction effects inherently present in studies of magnetization dynamics in large arrays of nanowires [38,39]. We develop an analytical model describing the spin wave frequencies in this system, and establish the boundary conditions for dynamic magnetization in Py wires studied in this work via comparison of the experimental data, analytical model, and micromagnetic simulation results.

II. EXPERIMENT

A series of Py(20–25 nm)/Pt(2 nm) wires of rectangular cross section such as that shown in Fig. 1(a) are patterned on top of a GaAs substrate via *e*-beam lithography, *e*-beam evaporation, and liftoff. The thin Pt capping layer is employed to prevent oxidation of the Py wire. Shorted coplanar strips (CPS) shown in Fig. 1(a) are patterned in close proximity to each wire and are used for application of a microwave
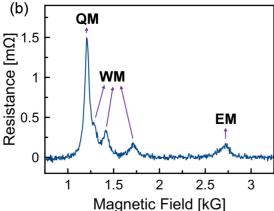
---

*justin.duan68@gmail.com

FIG. 1. (Color online) (a) Scanning electron micrograph of wire A. (b) FMR spectrum of wire B measured at the microwave drive frequency of 9 GHz. QM: quasiuniform mode; WM: width modes; EM: edge mode.

magnetic field H_{rf} to the wire. In this paper, we discuss three wire samples with similar Py thicknesses and different widths: (i) 1.18 μm × 25 nm (wire A), (ii) 620 nm × 25 nm (wire B), and (iii) 270 nm × 20 nm (wire C). The length of these wires is approximately 60 μm. We employ an electrically detected ferromagnetic resonance technique (FMR) [22] to study the spectral properties of spin wave eigenmodes of these samples as a function of magnetic field H applied in the plane of the sample perpendicular to the wire axis. In this technique, a microwave current I_{ac} in the CPS generates a microwave magnetic field nearly perpendicular to the sample plane at the nanowire location and excites spin wave eigenmodes in the Py wire when the frequency of I_{ac} coincides with its spin wave eigenmode frequencies. Excitation of the spin wave eigenmodes results in a small change δR in the time-average wire resistance that arises from anisotropic magnetoresistance (AMR) of Py [22,40,41]. This resistance variation is then measured as a function of H. Peaks in $\delta R(H)$ such as those shown in Fig. 1(b) represent the resonance fields of the spin wave eigenmodes.

The spin wave eigenmodes of in-plane transversely magnetized thin film ferromagnetic wires can be treated as width eigenmodes [22,30,42–44] due to the geometric confinement of the spin wave spectrum in the wire width direction. One particular mode that displays its maximum amplitude at the wire edges is called the edge mode (EM). Another mode that shows the lowest number of nodes along the wire width is

usually called the quasiuniform mode (QM). To simplify the discussion, the rest of the eigenmodes will be simply called width modes (WMs) throughout this paper. Figure 1(b) shows a typical FMR spectrum measured for wire B at the microwave drive frequency of 9 GHz. The peaks that appear at the lowest and highest fields are QM and EM [22,42,45,46], respectively. Between the two peaks a few width modes can also be clearly identified [30]. In our measurements, care was taken to keep the amplitude of I_{ac} small enough to remain within the linear regime of FMR. All measurements reported in this paper are performed at room temperature.

Figure 2 displays a color plot summary of FMR spectra such as that shown in Fig. 1(b) measured at multiple microwave drive frequencies. In this plot, the blue and red colors correspond to negative and positive values of δR, respectively. Figure 2 shows the dependence of spin wave mode frequencies on the applied field for all three samples studied in this work. This figure demonstrates that the frequency of each spin wave eigenmode exhibits a minimum as a function of the applied field. For a given sample, the frequency minimum is found at the same field H_b for all modes except EM. As we discuss below, H_b is the field, at which the magnetization in the interior of the wire becomes aligned along the applied field direction. Therefore, H_b can be called the bulk saturation field. Magnetization at the edges of the wire is more difficult to align with the external field because of the large demagnetizing field near the wire edges [47]. For this reason, the minimum frequency of the edge mode is achieved at the edge saturation field H_e that significantly exceeds H_b. For fields $H > H_b(H_e)$, the bulk (edge) spins become aligned with the applied field direction and the spin wave eigenmodes in this regime are called aligned width (edge) modes. For $H < H_b(H_e)$, the eigenmodes can be called nonaligned width (edge) modes.

III. THEORY

In order to analyze our experimental results, we develop a model describing the spin waves in transversely magnetized thin film wires. In this analytical model, we use a Cartesian coordinate system shown in the inset of Fig. 1(a), in which the external field is applied along the wire width $\vec{H} = H\hat{x}$. The cross section of the Py wire (excluding the Pt layer) has dimensions of $2a × 2b$, with $2b$ being the thickness and $b \ll a$. In our model, we make the following assumptions: (i) the applied field is strong enough that the wire in equilibrium is magnetized uniformly along the direction of the applied field, (ii) the wire is thin enough that the dynamic magnetization is considered uniform over the thickness (y axis), and (iii) the wire is long enough that translational invariance along the wire length (z axis) can be assumed. Assumptions (ii) and (iii) lead to the following form of magnetization of the wire driven by a small-amplitude alternating magnetic field with angular frequency ω: $\vec{M}(\vec{r},t) \simeq M_s\hat{x} + \text{Re}(\vec{m}_\omega(x)e^{-i\omega t})$, where M_s is the saturation magnetization of Py and $\vec{m}_\omega(x)$ is the amplitude of dynamic magnetization transverse to $\hat{x}$.

For the wires studied in this work, the first assumption of our model is met when the applied magnetic field exceeds the edge saturation field $H > H_e$. The second assumption is met because the thickness of the Py wire is comparable to the Py exchange length [48] and the frequencies of the spin wave
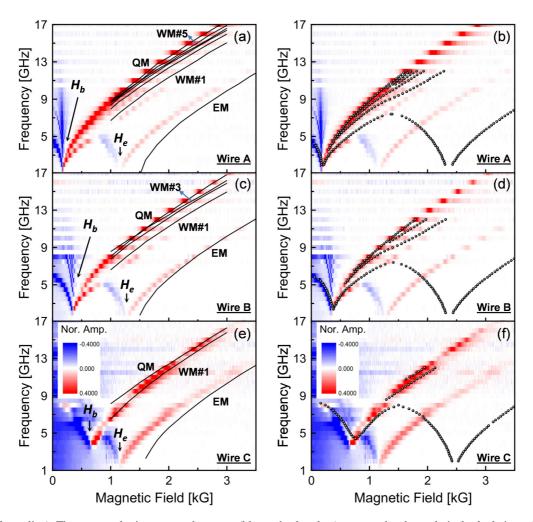
FIG. 2. (Color online) The measured spin wave mode spectra (blue-red color plots) compared to the analytical calculation using the partially pinned boundary condition [lines in (a), (c), and (e)] and to the micromagnetic simulation results [circles in (b), (d), and (f)]. (a),(b) Wire A; (c),(d) wire B; (e),(f) wire C.

eigenmodes discussed in our work are well below the lowest branch of perpendicular standing spin waves (PSSWs) [30,47]. The third assumption is met because the wavelength of the excited spin waves along the wire width is long (comparable to the CPS short length ~ 10 μm).

The starting point of our model is the Landau-Lifshitz (LL) equation:

$$\frac{d\vec{M}}{dt} = -|\gamma|\vec{M} \times \vec{H}_{\text{eff}}, \tag{1}$$

where γ is the gyromagnetic ratio and $\vec{H}_{\text{eff}}$ is the effective field defined as $\vec{H}_{\text{eff}} = \vec{H} + \vec{H}_D + \vec{H}_{\text{ex}}$, with $\vec{H}_D(\vec{M})$ and $\vec{H}_{\text{ex}} = (2A/M_s^2)\nabla^2\vec{M}$ being the demagnetizing field and the exchange field (A is the exchange stiffness), respectively. The linearized LL equation for the y and z components of the dynamic magnetization takes the form

$$iom_y^\omega = [h - n_x(x)]m_z^\omega - d\frac{\partial^2 m_z^\omega}{\partial x^2},$$

$$iom_z^\omega = -[h - n_x(x)]m_y^\omega + d\frac{\partial^2 m_y^\omega}{\partial x^2}$$
$$+ \langle\vec{h}_D(\vec{m})\rangle_y(x), \tag{2}$$

where $o \equiv (\omega/|\gamma|)/(4\pi M_s)$, $h \equiv H/(4\pi M_s)$, $n_x(x) \equiv -\langle\vec{H}_D(M_s\hat{x})\rangle_x/(4\pi M_s)$ is the x-dependent demagnetizing factor along $\hat{x}$, $\langle\vec{h}_D(\vec{m})\rangle_y(x) = \langle\vec{H}_D(\vec{m})\rangle_y(x)/(4\pi M_s)$ is the y component of the reduced dynamic demagnetizing field. Here $\langle\rangle$ denotes the average over the thickness, and $d \equiv A/(2\pi M_s^2) = l_{\text{ex}}^2$ (l_{ex} is the exchange length of Py).

The detailed derivation of the expressions for $n_x(x)$ and $\langle\vec{h}_D(\vec{m})\rangle_y(x)$ is given in the Appendix. Equation (2) together with boundary conditions for the dynamic magnetization set up an eigenvalue problem for the spin wave mode frequencies in the wire. The general form of the boundary conditions used for solving Eqs. (2) takes the following form [49,50]:

$$\left(\frac{\partial m_j}{\partial x} \pm \lambda m_j\right)_{x=\pm a} = 0 \qquad (j = x,y,z), \tag{3}$$

where λ is the parameter describing the partial pinning of the dynamic magnetization at the sample edge (the pinning parameter).

The value of the pinning parameter is determined by a number of factors, including the magnitude of magnetic surface anisotropy at the wire edge, edge roughness, edge surface profile, and the direction of magnetization with respect

to the edge normal [44]. For $\lambda = 0$, these boundary conditions reduce to the so-called free boundary conditions, which correspond to null normal derivatives of the magnetization at the edge surfaces. In this paper, we show that the free boundary conditions are appropriate for fully saturated transversely magnetized thin film wires without edge roughness, edge surface anisotropy, or irregular edge surface profiles (e.g., rounded or slanted edge surfaces). We also demonstrate that nonzero values of λ have to be used to quantitatively describe the experimental data (which implies non-negligible surface anisotropy, irregular edge surface profiles, and/or edge damage for our Py wires). Via comparison to the experimental data, we determine the value of λ appropriate for our system.

By representing the dynamic magnetization as a function of a specific Fourier series that satisfies the boundary conditions of Eq. (3) at the edges $x = \pm a$, the linearized Eq. (2) is reduced to a linear eigenvalue problem that can be easily solved by the standard linear algebra techniques as described in the Appendix. From these eigensolutions we obtain the frequencies and spatial profiles of the spin wave eigenmodes. We calculated the spin wave mode frequencies versus H for $H > H_e$ for several values of the pinning parameter λ, and found good agreement with the experimental data for all three samples for $\lambda = 0.05$ nm^{-1} as shown in Figs. 2(a), 2(c), and 2(e).

In order to test our analytical approach and gain understanding of the boundary conditions for the dynamic magnetization appropriate for our system, we performed micromagnetic simulations [51] of FMR spectra for the Py wires studied in this paper. The wires are divided to 1024 (along the length) $\times$ 256 (along the width) $\times$ 1 (along the thickness) cells. Since the dynamic magnetization is expected to be width dependent only, the numbers of cells along the wire length and thickness are not critical. In these simulations, we applied a spatially uniform continuous-wave magnetic drive field to the wire [52–54]. The simulation results were analyzed after the system had reached the dynamic equilibrium. The eigenmode resonance fields for a given drive frequency were extracted by examining the dependence of the dynamic magnetization amplitudes on the static external field.

The micromagnetic simulations also allow us to calculate the spectrum of nonaligned spin wave eigenmodes in the low-field regime ($H < H_e$). The aligned (nonaligned) spin wave modes can be clearly distinguished by the dependence of their frequencies on H [31]: the aligned mode frequency increases with H while the nonaligned mode frequency decreases with H. Therefore, the fields of the minimum frequency H_b and H_e mark transitions from the aligned to the nonaligned regimes of the spin wave modes. Figures 2(b), 2(d), and 2(f) compare the field dependence of spin wave eigenfrequencies obtained from the micromagnetic simulations to the experimental data for all three samples. It is clear from this figure that the micromagnetic simulations describe the spectrum of QM and WM with a high degree of accuracy. However, there are significant discrepancies for the edge mode. As we discuss in detail below, these discrepancies result from the extrinsic pinning of the dynamic magnetization at the wire edges by magnetic surface anisotropy, edge dilution, edge roughness, and/or irregular edge surfaces [44].

IV. RESULTS AND DISCUSSION

We employed our resistively detected FMR technique to measure the saturation magnetization M_s of each individual Py wire. As discussed in Ref. [22], M_s can be reliably determined via measurement of the quasiuniform mode frequency versus external field applied parallel to the wire axis. From these measurements we determined the saturation magnetization M_s of each wire: 790 ± 1 emu/cm^3 (wire A), 785 ± 1 emu/cm^3 (wire B), 850 ± 3 emu/cm^3 (wire C), which are typical for Py thin films [55–59]. These values of M_s together with a g-factor of 2.1 [59,60] and an exchange stiffness of 1.3 μerg/cm [55,57] are used as material parameters for our analytical calculations and micromagnetic simulations. We also note that the out-of-plane saturation field of our thin film wires was measured to be similar to $4\pi M_s$, which indicates that the Py/Pt interfacial anisotropy is small.

The analytical calculation typically provides a large number of eigensolutions that have spin wave mode profiles either symmetric or antisymmetric with respect to the wire center. We calculated the coupling coefficients of the microwave field profile [$< \pm 15\%$ amplitude variation across the widest wire as shown in Fig. 5(d)] to both types of modes and found that the coupling to the antisymmetric modes is one order of magnitude smaller than that to the symmetric modes. This makes the signal arising from excitation of the antisymmetric modes comparable to the noise level of our measurement. For this reason, we only consider the modes with symmetric mode profiles across the wire width throughout this paper.

Figure 3 provides a comparison of our micromagnetic simulations to the analytical calculations for the three studied wires. Analytical results for two values of the pinning parameter are shown: $\lambda = 0$ (free boundary conditions) and $\lambda = 0.05$ nm^{-1} (partially pinned boundary conditions). Both types of boundary conditions give similar eigenfrequencies for QM and WM, which are also similar to the micromagnetic simulation results and the experimental data (see Fig. 2). For the edge mode, however, the micromagnetic simulations only agree with the analytical calculation that employs the free boundary conditions. Since the simulations automatically account for the dipolar interaction at the wire edges, this indicates that the intrinsic dipolar edge pinning of spin waves [61] is negligible in transversely magnetized wires for the range of wire thicknesses and widths studied in present work. This is an important result as it proves that the free boundary conditions for the dynamic magnetization are appropriate for the description of spin wave eigenmodes in ideal (i.e., zero edge roughness, no edge dilution, zero surface anisotropy, and absence of rounding or slanting of the edge surfaces) ferromagnetic thin film wires that are transversely magnetized to full saturation. In other words, the edge pinning of magnetization in wires transversely magnetized to full saturation must have extrinsic character. This situation is to be contrasted with the case of ideal wires magnetized parallel to the wire edge, where demagnetizing fields lead to intrinsic partial pinning of the dynamic magnetization at the wire edges [61]. It has also been previously shown that the effective boundary conditions for wires that are not fully magnetized by a transverse magnetic field $H < H_e$ are different from the free boundary conditions [30]. Figures 3(c), 3(f), and 3(i)
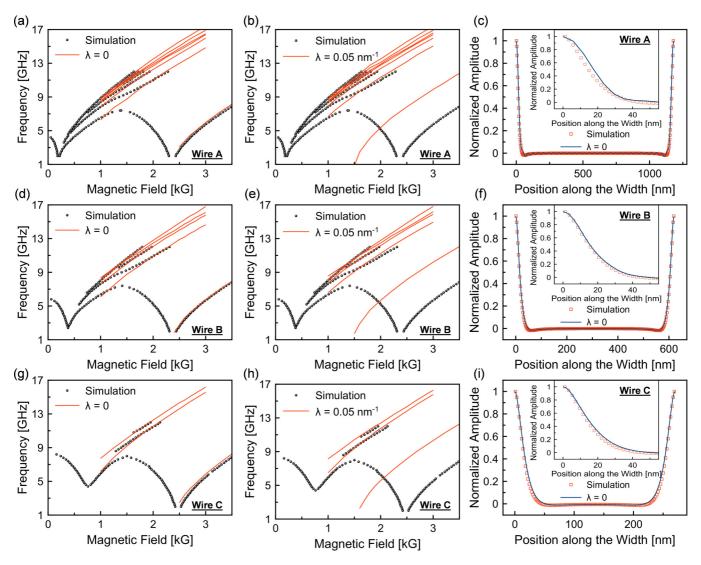
FIG. 3. (Color online) Comparison of spin wave eigenmodes calculated via the micromagnetic simulations (circles) to the analytical calculation (lines) using both boundary conditions: (a), (d), and (g) are free boundary conditions ($\lambda = 0$) for wires A, B, and C respectively; (b), (e), and (h) are partially pinned boundary conditions ($\lambda = 0.05$ nm^{-1}) for wires A, B, and C respectively. Panels (c), (f), and (i) show the edge spin wave mode spatial profiles along the wire width at $H = 2.7$ kG for wires A, B, and C respectively. Blue solid line: analytical calculation using free boundary conditions ($\lambda = 0$); red open squares: micromagnetic simulations. The insets show the zoom-in view near the wire edges.

compare the edge spin wave mode profiles in the studied wires calculated analytically with the free boundary conditions ($\lambda = 0$) to the profiles given by micromagnetic simulations. The nearly perfect agreement between the two approaches also lends support to our conclusion that the free boundary conditions are appropriate for transversely magnetized wires for the range of wire thicknesses and widths studied in this work.

The left panel of Fig. 2 compares the experimentally measured FMR eigenmodes to the analytical calculation using the partially pinned boundary condition with $\lambda = 0.05$ nm^{-1}. The calculated frequencies of all eigenmodes are in good agreement with the experimental data, especially in the high-field limit. This is illustrated in Fig. 4, which compares the measured eigenmode frequencies to those calculated by using the free and the partially pinned boundary conditions for wire B at $H = 2.7$ kG. It is also clear from this figure that the

free boundary conditions fail to describe the edge mode, and, therefore, extrinsic edge pinning must be invoked to explain the experimental data.

Figure 5 shows the spin wave mode profiles (spatial dependencies of the mode amplitudes across the wire width) calculated for both the free ($\lambda = 0$) and the partially pinned ($\lambda = 0.05$ nm^{-1}) boundary conditions at $H = 2.7$ kG. The general behavior of the spin wave mode profiles is a gradual shift of the maximum spin wave amplitude from the wire center towards the wire edge with decreasing mode frequency. We also note that there is no direct correlation between the mode index and the number of nodes in the mode profile along the wire width, which is a consequence of the complex interplay between the exchange and dipolar interactions for these spin waves. It is clear from Fig. 5 that the edge pinning ($\lambda > 0$) increases the curvature of the mode profiles near the edges, which leads to increase of the exchange energy
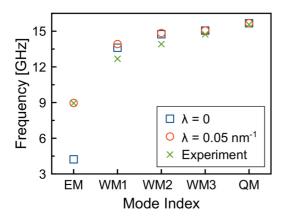
FIG. 4. (Color online) Spin wave eigenfrequencies for wire B at $H = 2.7$ kG: experiment (crosses), free boundary conditions (squares), and partially pinned boundary conditions (circles). EM: edge mode; QM: quasiuniform mode; WM1–WM3: width modes with increasing frequencies.

and the associated increase in the mode frequency. Figure 4 clearly shows that the mode frequency difference between the free and partially pinned boundary conditions increases with decreasing mode frequency, which results from the shift of the mode profile towards the wire edge.

The dependence of the spin wave eigenmode properties on the wire width is best exemplified by the quasiuniform and the edge modes. Figure 6(a) shows the dependence of the bulk saturation field H_b and the quasiuniform mode frequency on the wire width. This figure demonstrates that

the bulk saturation field rapidly increases with decreasing wire width. This increase in H_b results from the increase of the demagnetizing field inside the wire. Figure 6(b) shows the spatial profile of the demagnetizing field $4\pi M_s n_x(x)$ in the wire interior as derived in the Appendix. It is clear from this figure that the bulk saturation field shown in Fig. 6(a) is similar to the demagnetizing field in the center region of the wire. For a given value of the applied field, the higher demagnetizing field in narrower wires results in a smaller net magnetic field in the wire interior, and hence leads to lower spin wave mode frequencies in narrower wires as shown in Fig. 6(a).

While the demagnetizing field is a strong function of the wire width in the center region of the wire, it is nearly width independent at the wire edge as illustrated in Fig. 6(c). For this reason, the edge saturation field H_e is expected to be nearly independent on the wire width. This indeed is the case as shown in Fig. 7(a). Since the edge demagnetizing field profile is nearly independent on the wire width, the edge mode frequencies and spatial profiles are also expected to be the same. Figure 7(a) shows that both the measured and the calculated edge mode frequencies are indeed nearly independent on the wire width.

While taking into account extrinsic pinning is needed to explain the observed frequencies of the edge mode, we expect this extrinsic pinning to be nearly the same for all three wire samples studied because these wires were prepared via the same fabrication protocol. This is indeed the case, because the same pinning parameter ($\lambda = 0.05$ nm^{-1}) gives the eigenfrequency values very similar to those observed in the experiment. Figures 7(b) and 7(c) show the calculated edge

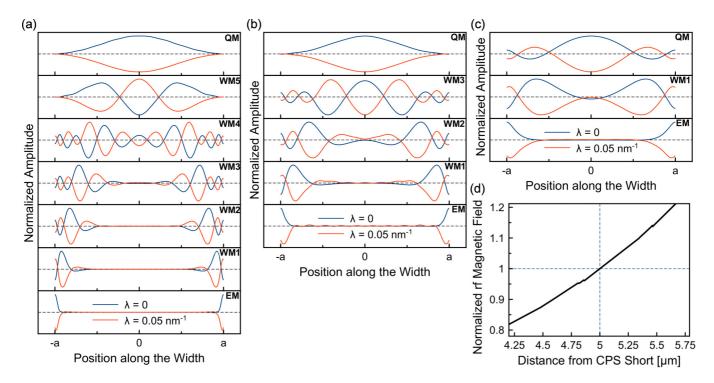FIG. 5. (Color online) Spin wave mode spatial profiles along the wire width at $H = 2.7$ kG for wire A (a), wire B (b), and wire C (c). EM: edge mode; QM: quasiuniform mode; WM1–WM5: width spin wave modes with increasing frequencies. Blue and red traces represent the free ($\lambda = 0$) and the partially pinned boundary conditions ($\lambda = 0.05$ nm^{-1}). For clarity, the phases of the mode profiles for the two boundary conditions are chosen to be opposite. (d) Reduced amplitude of the applied microwave magnetic field from CPS along the wire width (x axis).
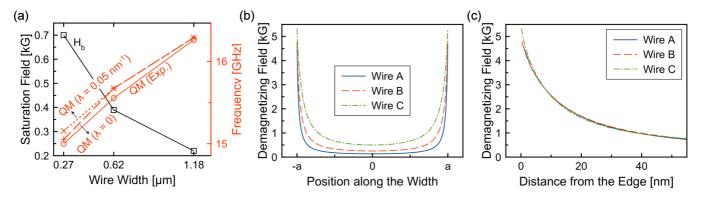
FIG. 6. (Color online) (a) The measured bulk saturation fields H_b (open squares), measured (open circles), and calculated (crosses) quasiuniform mode eigenfrequencies as a function of the wire width. The calculated spatial profiles of the demagnetizing field at $H = 2.7$ kG across the wire width (b) and at the wire edge (c).

mode profiles for the free and the partially pinned boundary conditions. These figures illustrate that the edge mode profiles are indeed nearly independent on the wire width for both types of the boundary conditions used in this study.

It is important to note that the maximum demagnetizing field occurs at the wire edges [$\sim 2\pi M_s$, see Fig. 6(c)] and is larger than the calculated edge saturation field assuming ideal wires with no extrinsic edge pinning ($2.4 \sim 2.5$ kG; see Fig. 3). In other words, for an external field not too much larger than the edge saturation field H_e, there is a small region near the wire edges where the net field opposes the external field. The length scale of this region is comparable to the exchange length [see Fig. 6(c)]. The negative net field will not cause noticeable misalignment of the edge spins from the external field, which otherwise would introduce a significant exchange energy increase. As a result, the equilibrium magnetization is stabilized by the exchange interaction close to edges, as also noted in Ref. [44]. In nonideal wires, extrinsic parameters such as the edge surface anisotropy also play a stabilizing role for the equilibrium magnetization.

In summary, we present detailed experimental and theoretical studies of spin wave eigenmodes in transversely magnetized thin film Py wires as a function of the wire width. Using resistively detected ferromagnetic resonance technique, we measure the spectrum of spin waves in individual Py wires

as a function of magnetic field applied perpendicular to the wire axis. We observe several spin wave modes and compare their frequencies to the predictions of our analytical model and micromagnetic simulations. Comparison of the analytical model and micromagnetic simulations demonstrates that the free boundary conditions for dynamic magnetization provide an adequate description of the spin wave eigenmode spectrum in transversely magnetized wires in the absence of extrinsic edge pinning. Comparison of our theoretical model to the measured spin wave frequencies reveals that the extrinsic edge pinning is present at the wire edges and that the pinning parameter $\lambda \approx 0.05$ nm^{-1} is nearly independent on the wire width. Using our analytical model, we calculate the spin wave mode profiles across the nanowire width and show how the maximum of the mode amplitude progressively shifts from the wire center to the wire edge as a function of the eigenmode frequency. We find that the frequency of the quasiuniform mode decreases with decreasing width of the wire while the frequency of the edge mode is nearly independent of the wire width. These trends are explained by the width dependence of the static demagnetizing fields in the bulk of the wire and near the wire edges. Our work establishes the boundary conditions for the dynamic magnetization for transversely magnetized thin film Py wires for the range of wire thicknesses and widths studied, and provides quantitative explanation of the spin wave
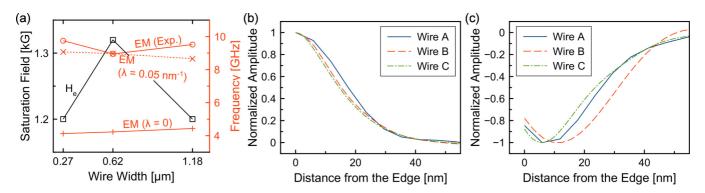

FIG. 7. (Color online) (a) The measured edge saturation field H_e (open squares), measured (open circles) and calculated (crosses) edge mode eigenfrequencies at $H = 2.7$ kG as a function of the wire width. Edge modes spatial profiles at $H = 2.7$ kG for (b) free ($\lambda = 0$) and (c) partially pinned ($\lambda = 0.05$ nm^{-1}) boundary conditions.

eigenmode frequencies and spatial profiles in this system as a function of the wire width.

APPENDIX

In this section, we present the solution of the spin wave eigenvalue problem based on the linearized Landau-Lifshitz given by Eq. (2).

We start by calculating the static demagnetizing field $\vec{H}_D(M_s\hat{x})$ produced by the equilibrium magnetization saturated in the sample plane perpendicular to the wire axis, $M_s\hat{x}$. More specifically, we calculate the x component of the demagnetizing field averaged over the film thickness $\langle\vec{H}_D(M_s\hat{x})\rangle(x)$. This demagnetizing field can be calculated as a derivative of a magnetostatic scalar potential $\phi(x,y)$:

$$\langle\vec{H}_D(M_s\hat{x})\rangle(x) = -\left\langle\frac{\partial\phi}{\partial x}\right\rangle\hat{x} = -4\pi M_s n_x(x)\hat{x}, \quad (A1)$$

where $n_x(x)$ is the spatially dependent demagnetizing factor. The magnetostatic potential is z independent due to z axis translational invariance of the system.

The potential $\phi(x,y)$ is generated by magnetic charges of density $\pm M_s$ located at the wire edges ($x' = \pm a$). By using the well-known expression for the potential created by an infinite (in the z direction) line of charges located at (x',y'): $\tilde{\phi}(x,y) = -2\Lambda\ln\sqrt{(y-y')^2+(x-x')^2}$, where Λ is the linear magnetic charge density, we can write down an expression for the potential generated by each of the two edges of the wire:

$$\phi_{\pm}(x,y) = -2\Lambda\int_{-b}^{b}dy'\ln\sqrt{(y-y')^2+(x\pm a)^2}. \quad (A2)$$

By averaging over the wire thickness and taking a derivative with respect to x, we obtain an expression for the effective demagnetizing field generated by each wire edge:

$$-\left\langle\frac{\partial\phi_{\pm}}{\partial x}\right\rangle\hat{x} = \hat{x}\frac{\Lambda}{b}\int_{-b}^{b}dy\int_{-b}^{b}dy'\frac{(x\pm a)}{(y-y')^2+(x\pm a)^2}. \quad (A3)$$

Evaluating the integrals in Eq. (A3), we obtain an exact analytical expression for the demagnetizing

factor $n_x(x)$ [62]:

$$n_x(x) = \frac{1}{\pi}\Big\{\tan^{-1}[2p/(1+X)] + \tan^{-1}[2p/(1-X)]\Big\}$$

$$+ \frac{1}{4\pi p}\Bigg[(1+X)\ln\left(\frac{(1+X)^2}{(2p)^2+(1+X)^2}\right)$$

$$+ (1-X)\ln\left(\frac{(1-X)^2}{(2p)^2+(1-X)^2}\right)\Bigg], \quad (A4)$$

where $X \equiv x/a$ and $p \equiv b/a$.

The dynamic demagnetizing field $\langle\vec{H}_D(\vec{m}_\omega)\rangle$ produced by the dynamic magnetization $\vec{m}_\omega$ and its average over the nanowire thickness can be calculated using the reciprocity theorem [63]. We start by averaging the dynamic demagnetizing field (for example, its y component) over the section of the wire of width Δx (and of volume $\Delta V_{(x)} = 2b\Delta x\Delta z$) evaluated at x:

$$\langle\vec{H}_D(\vec{m}_\omega)\rangle_y(x) = \frac{1}{\Delta V_{(x)}}\int_{\Delta V_{(x)}}dV'\vec{H}_D(\vec{m}_\omega)\cdot\hat{y}. \quad (A5)$$

Using the reciprocity theorem, this expression can be written in the following form:

$$\langle\vec{H}_D(\vec{m}_\omega)\rangle_y(x) = \frac{1}{\Delta V_{(x)}}\int_V dV'\vec{H}_D(\hat{y}^{(x)})(x')\cdot\vec{m}_\omega(x')$$

$$= -\frac{1}{2b\Delta x}\int_{-a}^{a}dx'\Delta\phi^{\hat{y}^{(x)}}(x')m_y(x'), \quad (A6)$$

where $\hat{y}^{(x)}$ is defined as an "auxiliary" magnetization restricted to the Δx section located at x and $\Delta\phi^{\hat{y}^{(x)}}(x')$ is given by

$$\Delta\phi^{\hat{y}^{(x)}}(x') = -4\Delta x\ln\left(\frac{|x-x'|}{\sqrt{(x-x')^2+(2b)^2}}\right). \quad (A7)$$

This leads to

$$\langle\vec{H}_D(\vec{m}_\omega)\rangle_y(x)$$

$$= -\frac{1}{p}\int_{-1}^{1}dX'm_y(X')\ln\{1+[2p/(X-X')]^2\}. \quad (A8)$$

The reduced dynamic demagnetizing field in Eq. (2) is given by $\langle\vec{h}_D(\vec{m})\rangle_y(x) = \langle\vec{H}_D(\vec{m}_\omega)\rangle_y(x)/(4\pi M_s)$.

We first solve the spin wave eigenmode problem for the case of free boundary conditions $\partial m_{y,z}/\partial x(\pm a) = 0$. The eigenvalue integrodifferential equations in Eq. (2) can be solved by introducing a Fourier series representation for the dynamic magnetization that satisfies the boundary conditions ($\partial m_{y,z}/\partial X = 0$ at $X = \pm 1$, i.e., at the wire edges):

$$m_y(X) = A_0 + \sum_{l=1}^{L}\{A_l\cos(l\pi X) + B_l\sin[(2l-1)\pi X/2]\},$$

$$m_z(X) = C_0 + \sum_{l=1}^{L}\{C_l\cos(l\pi X) + D_l\sin[(2l-1)\pi X/2]\}.$$

$$(A9)$$

The integrodifferential equations in Eq. (2) then become the problem of solving the eigenvalue matrix equations for the coefficients of the Fourier expansions. There are independent

equations for the symmetric modes,

$$ioA_0 = (h_o - ncc_{00}/2)C_0 - ncc_{0l}C_l/2,$$
$$ioC_0 = -(h_o - ncc_{00}/2)A_0 + ncc_{0l}A_l/2$$
$$+ (cc_{00}A_0 + cc_{0l}A_l)/4\pi p,$$
$$ioA_n = [h_o + d(n\pi/a)^2]C_n - ncc_{nl}C_l,$$
$$ioC_n = -[h_o + d(n\pi/a)^2]A_n + ncc_{nl}A_l$$
$$+ (cc_{n0}A_0 + cc_{nl}A_l)/2\pi p, \tag{A10}$$

and for the antisymmetric modes,

$$ioB_n = \{h_o + d[(2n-1)\pi/2a]^2\}D_n - nss_{nl}D_l,$$
$$ioD_n = -\{h_o + d[(2n-1)\pi/2a]^2\}B_n + nss_{nl}B_l$$
$$+ ss_{nl}B_l/2\pi p. \tag{A11}$$

In these equations, the Einstein summation convention is used and the coefficients are given by the following expressions:

$$ncc_{nl} \equiv \int_{-1}^{1} dX n_x(X) \cos(n\pi X) \cos(l\pi X),$$

$$nss_{nl} \equiv \int_{-1}^{1} dX n_x(X) \sin[(2n-1)\pi X/2] \sin[(2l-1)\pi X/2],$$

$$cc_{nl} \equiv \int_{-1}^{1} dX' \int_{-1}^{1} dX \ln\left(\frac{|X - X'|}{\sqrt{(X - X')^2 + (2p)^2}}\right)$$
$$\times \cos(n\pi X') \cos(l\pi X)$$

$$ss_{nl} \equiv \int_{-1}^{1} dX' \int_{-1}^{1} dX \ln\left(\frac{|X - X'|}{\sqrt{(X - X')^2 + (2p)^2}}\right)$$
$$\times \sin[(2n-1)\pi X'/2] \sin[(2l-1)\pi X/2]. \tag{A12}$$

In the case of partially pinned boundary conditions given by Eq. (3), a similar Fourier series that guarantees satisfaction of the boundary conditions was used:

$$m_y(X) = \sum_n \left[A_n \cos\left(\kappa_n^s X\right) + B_n \sin\left(\kappa_n^a X\right)\right],$$
$$m_z(X) = \sum_n \left[C_n \cos\left(\kappa_n^s X\right) + D_n \sin\left(\kappa_n^a X\right)\right], \tag{A13}$$

with the wave vectors $\kappa_n^{(s,a)}$ obtained by solving the following transcendental equations:

$$\tan\left(\kappa_n^s\right) = (\lambda a)\kappa_n^s,$$
$$\cot\left(\kappa_n^a\right) = -(\lambda a)\kappa_n^a. \tag{A14}$$

[1] T. Koyama *et al.*, Nat. Nanotechnol. **7**, 635 (2012).

[2] A. J. Schellekens, A. van den Brink, J. H. Franken, H. J. M. Swagten, and B. Koopmans, Nat. Commun. **3**, 847 (2012).

[3] M. Kläui, P.-O. Jubert, R. Allenspach, A. Bischof, J. A. C. Bland, G. Faini, U. Rudiger, C. A. F. Vaz, L. Vila, and C. Vouille, Phys. Rev. Lett. **95**, 026601 (2005).

[4] I. M. Miron *et al.*, Nat. Mater. **10**, 419 (2011).

[5] A. Chanthbouala *et al.*, Nat. Phys. **7**, 626 (2011).

[6] S.-H. Yang, K.-S. Ryu, and S. Parkin, Nat. Nanotechnol. **10**, 221 (2015).

[7] C. T. Boone and I. N. Krivorotov, Phys. Rev. Lett. **104**, 167205 (2010).

[8] C. Hassel, M. Brands, F. Y. Lo, A. D. Wieck, and G. Dumpich, Phys. Rev. Lett. **97**, 226805 (2006).

[9] A. Aziz, S. J. Bending, H. G. Roberts, S. Crampin, P. J. Heard, and C. H. Marrows, Phys. Rev. Lett. **97**, 206602 (2006).

[10] L. K. Bogart and D. Atkinson, Appl. Phys. Lett. **94**, 042511 (2009).

[11] L. Bocklage, S. Motl-Ziegler, J. Topp, T. Matsuyama, and G. Meier, J. Phys.: Condens. Matter **26**, 266003 (2014).

[12] S. Choi, K.-S. Lee, K. Y. Guslienko, and S.-K. Kim, Phys. Rev. Lett. **98**, 087205 (2007).

[13] M. Mochizuki, Phys. Rev. Lett. **108**, 017601 (2012).

[14] H. F. Du, J. P. DeGrave, F. Xue, D. Liang, W. Ning, J. Y. Yang, M. L. Tian, Y. H. Zhang, and S. Jin, Nano Lett. **14**, 2026 (2014).

[15] A. Fert, V. Cros, and J. Sampaio, Nat. Nanotechnol. **8**, 152 (2013).

[16] J. Sampaio, V. Cros, S. Rohart, A. Thiaville, and A. Fert, Nat. Nanotechnol. **8**, 839 (2013).

[17] R. Tomasello, E. Martinez, R. Zivieri, L. Torres, M. Carpentieri, and G. Finocchio, Sci. Rep. **4**, 6784 (2014).

[18] L. Vila, T. Kimura, and Y. C. Otani, Phys. Rev. Lett. **99**, 226604 (2007).

[19] Z. Duan, A. Smith, L. Liu, B. Youngblood, J. Lindner, V. E. Demidov, S. O. Demokritov, and I. N. Krivorotov, Nat. Commun. **5**, 5616 (2014).

[20] L. Liu, C.-F. Pai, D. C. Ralph, and R. A. Buhrman, Phys. Rev. Lett. **109**, 186602 (2012).

[21] L. Liu, C.-F. Pai, Y. Li, H. W. Tseng, D. C. Ralph, and R. A. Buhrman, Science **336**, 555 (2012).

[22] Z. Duan, C. T. Boone, X. Cheng, I. N. Krivorotov, N. Reckers, S. Stienen, M. Farle, and J. Lindner, Phys. Rev. B **90**, 024427 (2014).

[23] D. A. Allwood, G. Xiong, C. C. Faulkner, D. Atkinson, D. Petit, and R. P. Cowburn, Science **309**, 1688 (2005).

[24] J. Jaworowicz, N. Vernier, J. Ferré, A. Maziewski, D. Stanescu, D. Ravelosona, A. S. Jacqueline, C. Chappert, B. Rodmacq, and B. Diény, Nanotechnology **20**, 215401 (2009).

[25] S. Dutta, S.-C. Chang, N. Kani, D. E. Nikonov, S. Manipatruni, I. A. Young, and A. Naeemi, Sci. Rep. **5**, 9861 (2015).

[26] A. Khitun, and K. Wang, J. Appl. Phys. **110**, 034306 (2011).

[27] A. Khitun, J. Appl. Phys. **111**, 054307 (2012).

[28] S. Klingler, P. Pirro, T. Brächer, B. Leven, B. Hillebrands, and A. V. Chumak, Appl. Phys. Lett. **105**, 152410 (2014).

[29] V. E. Demidov and S. O. Demokritov, IEEE Trans. Magn. **51**, 1 (2015).

[30] C. Bayer, J. Jorzick, S. O. Demokritov, A. N. Slavin, K. Y. Guslienko, D. V. Berkov, N. L. Gorn, M. P. Kostylev, and B. Hillebrands, Top. Appl. Phys. **101**, 57 (2006).

[31] H. T. Nguyen, T. M. Nguyen, and M. G. Cottam, Phys. Rev. B **76**, 134413 (2007).

[32] E. Meloche, J. I. Mercer, J. P. Whitehead, T. M. Nguyen, and M. L. Plumer, Phys. Rev. B **83**, 174425 (2011).

[33] M. V. Costache, S. M. Watts, M. Sladkov, C. H. van der Wal, and B. J. van Wees, Appl. Phys. Lett. **89**, 232115 (2006).

[34] K. Ando, J. Ieda, K. Sasage, S. Takahashi, S. Maekawa, and E. Saitoh, Appl. Phys. Lett. **94**, 262505 (2009).

[35] C. T. Boone, J. A. Katine, J. R. Childress, V. Tiberkevich, A. Slavin, J. Zhu, X. Cheng, and I. N. Krivorotov, Phys. Rev. Lett. **103**, 167601 (2009).

[36] A. A. Tulapurkar, Y. Suzuki, A. Fukushima, H. Kubota, H. Maehara, K. Tsunekawa, D. D. Djayaprawira, N. Watanabe, and S. Yuasa, Nature (London) **438**, 339 (2005).

[37] J. C. Sankey, P. M. Braganca, A. G. F. Garcia, I. N. Krivorotov, R. A. Buhrman, and D. C. Ralph, Phys. Rev. Lett. **96**, 227601 (2006).

[38] G. Gubbiotti, S. Tacchi, G. Carlotti, P. Vavassori, N. Singh, S. Goolaup, A. O. Adeyeye, A. Stashkevich, and M. Kostylev, Phys. Rev. B **72**, 224413 (2005).

[39] B. Hillebrands and K. Ounadjela, *Spin Dynamics in Confined Magnetic Structures II* (Springer, New York, 2003).

[40] C. Wang, Y.-T. Cui, J. Z. Sun, J. A. Katine, R. A. Buhrman, and D. C. Ralph, Phys. Rev. B **79**, 224416 (2009).

[41] N. Mecking, Y. S. Gui, and C.-M. Hu, Phys. Rev. B **76**, 224430 (2007).

[42] J. Jorzick, S. O. Demokritov, B. Hillebrands, M. Bailleul, C. Fermon, K. Y. Guslienko, A. N. Slavin, D. V. Berkov, and N. L. Gorn, Phys. Rev. Lett. **88**, 047204 (2002).

[43] J. P. Park, P. Eames, D. M. Engebretson, J. Berezovsky, and P. A. Crowell, Phys. Rev. Lett. **89**, 277201 (2002).

[44] R. D. McMichael and B. B. Maranville, Phys. Rev. B **74**, 024424 (2006).

[45] P. S. Keatley, V. V. Kruglyak, A. Neudert, E. A. Galaktionov, R. J. Hicken, J. R. Childress, and J. A. Katine, Phys. Rev. B **78**, 214412 (2008).

[46] E. K. Semenova *et al.*, Phys. Rev. B **87**, 174432 (2013).

[47] C. Bayer, S. O. Demokritov, B. Hillebrands, and A. N. Slavin, Appl. Phys. Lett. **82**, 607 (2003).

[48] A. Guimarães, *Priniciples of Nanomagnetism* (Springer, New York, 2009).

[49] G. T. Rado and J. R. Weertman, J. Phys. Chem. Solids **11**, 315 (1959).

[50] R. F. Soohoo, Phys. Rev. **131**, 594 (1963).

[51] A. Vansteenkiste, J. Leliaert, M. Dvornik, M. Helsen, F. Garcia-Sanchez, and B. van Waeyenberge, AIP Adv. **4**, 107133 (2014).

[52] C. Schoeppner, K. Wagner, S. Stienen, R. Meckenstock, M. Farle, R. Narkowicz, D. Suter, and J. Lindner, J. Appl. Phys. **116**, 033913 (2014).

[53] A. Banholzer, R. Narkowicz, C. Hassel, R. Meckenstock, S. Stienen, O. Posth, D. Suter, M. Farle, and J. Lindner, Nanotechnology **22**, 295713 (2011).

[54] K. Wagner, S. Stienen, and M. Farle, arXiv:1506.05292.

[55] G. Gubbiotti *et al.*, Phys. Rev. B **90**, 024419 (2014).

[56] J. O. Rantschler, P. J. Chen, A. S. Arrott, R. D. McMichael, W. F. Egelhoff Jr., and B. B. Maranville, J. Appl. Phys. **97**, 10J113 (2005).

[57] S. Jung, B. Watkins, L. DeLong, J. B. Ketterson, and V. Chandrasekhar, Phys. Rev. B **66**, 132401 (2002).

[58] J. J. Ding, G. N. Kakazei, X. M. Liu, K. Y. Guslienko, and A. O. Adeyeye, Sci. Rep. **4**, 4796 (2014).

[59] J. P. Nibarger, R. Lopusnik, Z. Celinski, and T. J. Silva, Appl. Phys. Lett. **83**, 93 (2003).

[60] J. M. Shaw, H. T. Nembach, T. J. Silva, and C. T. Boone, J. Appl. Phys. **114**, 243906 (2013).

[61] K. Y. Guslienko, S. O. Demokritov, B. Hillebrands, and A. N. Slavin, Phys. Rev. B **66**, 132402 (2002).

[62] R. I. Joseph and E. Schlömann, J. Appl. Phys. **36**, 1579 (1965).

[63] W. F. Brown, Jr., *Micromagnetics* (Wiley, New York, 1963).